

# CleverDistiller: Simple and Spatially Consistent Cross-modal Distillation

Hariprasath Govindarajan<sup>2\*</sup>  
Camille Maurice<sup>1</sup>

Maciej K. Wozniak<sup>1,5\*</sup>  
B Ravi Kiran<sup>3</sup>  
Senthil Yogamani<sup>4</sup>

\*co-first authors

{mwozniak, hargov, mklingne, cmaurice, ravgira, syogaman}@qti.qualcomm.com

<sup>1</sup>Qualcomm Arriver Software GmbH

<sup>2</sup>Qualcomm Auto Ltd Sweden Filial and Linköping University, Sweden

<sup>3</sup>Qualcomm France, S.A.R.L.    <sup>4</sup>Qualcomm Technologies, Inc.

<sup>5</sup>KTH Royal Institute of Technology, Sweden

## Abstract

*Vision foundation models (VFs) such as DINO have led to a paradigm shift in 2D camera-based perception towards extracting generalized features to support many downstream tasks. Recent works introduce self-supervised cross-modal knowledge distillation (KD) as a way to transfer these powerful generalization capabilities into 3D LiDAR-based models. However, they either rely on highly complex distillation losses, pseudo-semantic maps, or limit KD to features useful for semantic segmentation only. In this work, we propose **CleverDistiller**, a self-supervised, cross-modal 2D-to-3D KD framework introducing a set of simple yet effective design choices: Unlike contrastive approaches relying on complex loss design choices, our method employs a direct feature similarity loss in combination with a multi layer perceptron (MLP) projection head to allow the 3D network to learn complex semantic dependencies throughout the projection. Crucially, our approach does not depend on pseudo-semantic maps, allowing for direct knowledge transfer from a VFM without explicit semantic supervision. Additionally, we introduce the auxiliary self-supervised spatial task of occupancy prediction to enhance the semantic knowledge, obtained from a VFM through KD, with 3D spatial reasoning capabilities. Experiments on standard autonomous driving benchmarks for 2D-to-3D KD demonstrate that CleverDistiller achieves state-of-the-art performance in both semantic segmentation and 3D object detection (3DOD) by up to 10% mIoU, especially when fine tuning on really low data amounts, showing the effectiveness of our simple yet powerful KD strategy.*

## 1. Introduction

For many vision applications such as autonomous driving, research is focused on improving generalized understand-

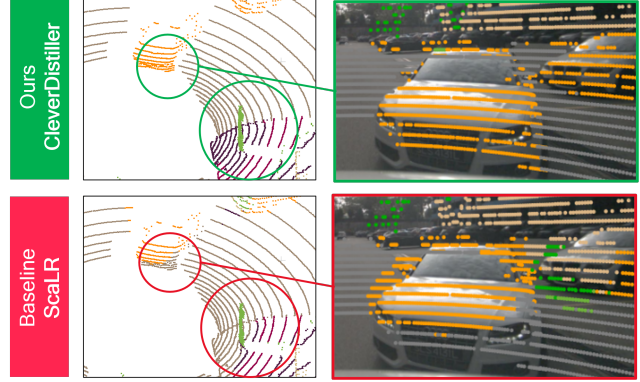


Figure 1. We observe how **CleverDistiller** (top) improves over the baseline ScaLR (bottom). 3D representations from both KD methods are fine-tuned to the 3D semantic segmentation task on nuScenes. We observe how our approach encourages spatially consistent semantic outputs.

ing of the environment to increase safety and autonomy. However, constant updates of sensor types and setups from different manufacturers makes it difficult to train one perception system that excels on all use cases. Most perception models for, e.g., object detection or semantic segmentation, are known for their lack of robustness towards weather conditions, lighting, sensor setup, or driving environments that usually deviate between inference and training. Especially, LiDAR-based 3D models are known for their adaptation challenges [2, 26, 34, 41, 47, 55, 59, 67, 70–72, 82, 85, 86, 89].

Due to these inherent difficulties in adaptation, recent focus has shifted towards using VFs such as DINO [36, 54]. These models provide features that are robust to different sensor setups and environments, while being able to support multiple downstream tasks [12, 45, 63, 73]. While many works address and extend VFs in camera-based setups,

our work is aimed at transferring VFM knowledge to more challenging LiDAR-based 3D networks. In this direction, cross-modal knowledge distillation has been used to transfer learned feature representations between the backbones of different sensor modalities. Initial methods focused mainly on distilling LiDAR-based features into camera-based models [18, 38]. However, with the emergence of VFMs the reverse direction, to distill generalized semantic 2D features into 3D LiDAR-based networks, has become highly relevant [49, 57, 83, 84]. While initial work is mostly focused on 3D semantic segmentation as a downstream task, we aim to obtain a pre-trained LiDAR-based backbone that can be applied to various downstream tasks, e.g., both 3D semantic segmentation and 3DOD.

Many previous approaches for cross-modal KD have tried to explicitly model the semantic dependencies by using semantic priors (generated by e.g., Segment Anything (SAM) or OpenSeeD [37, 83, 84, 90, 92]) and auxiliary spatial tasks. Although showing improvements in performance and robustness, these approaches tend to complicate the cross-modal KD process. Therefore, we build on the second type of approach presented by ScaLR [57] which proposes a simple distillation solution, however, without achieving SOTA performance. As demonstrated in Fig. 1 ScaLR often yields semantic outputs that are not consistent with the scene’s spatial structure.

To address these shortcomings, we propose **CleverDistiller**, a fully self-supervised KD framework that transfers features from a camera-based VFM to a LiDAR-based 3D network. Our approach relies on a multi-task feature distillation strategy that integrates cross-modal KD from a VFM and an auxiliary spatial task, i.e., occupancy prediction [8], to capture both semantic and spatial information in a unified framework, thereby improving spatial and semantic feature consistency, cf. Fig. 1. Our contributions can be summarized as follows:

- We identify linear projection of 3D LiDAR features into 2D space of camera-based VFM features as the main limitation of simple cross-modal KD loss functions. We therefore introduce an MLP projection head on top of the 3D LiDAR backbone to allow flexible learning of 3D spatial properties in the distillation between structurally very different 2D image and 3D LiDAR features while retaining simplicity on the distillation loss from VFM features.
- We also incorporate the auxiliary self-supervised task of occupancy prediction to preserve spatial information within the LiDAR model. Thereby, generalized semantic features distilled from the VFM are further encouraged to be spatially consistent across the 3D scene.
- We demonstrate that CleverDistiller outperforms previous approaches in standard 2D-to-3D KD benchmarks for both 3D semantic segmentation and 3DOD. Our model is particularly successful when fine-tuned on low amount-

of data, highlighting the generalization capabilities of our learned 3D features.

## 2. Related work

**Pre-training Vision Models:** Supervised pre-training on large labeled datasets [21, 31, 44, 65, 66] has being replaced by self-supervised pre-training [25]. Self-supervised pre-training involves training a model using a pretext task on large unlabeled datasets. Currently, self-supervised learning (SSL) methods predominantly use a contrastive [14] or reconstruction formulation [54, 96]. Initially, a contrastive objective was considered over data instances in a batch [14, 78] or a memory bank [15, 16, 32]. Recent works such as DINO [12] contrast over prototypical clusters [3, 10, 11, 29, 46] and learn representations that are highly data efficient [4, 58]. Reconstruction based methods [6, 33] typically lack data efficiency [5]. Then, DINOv2 [54] consolidated a range of strategies such as masked image modeling [96] and produced a model that excels on a wide range of downstream tasks, adopted in many recent works [24, 30, 68]. In this work we also adopt DINOv2 as a teacher model to train a 3D student backbone through pixel-to-point correspondence of features. While pre-training models on the target domain is a promising direction [45, 73], there is a lack of off-the-shelf models for autonomous driving, of a similar quality to DINOv2.

**Pre-training 3D Backbones** Self-supervised pre-training of 3D backbones started with single object scans (e.g. ShapeNet [13, 77]) similar to ImageNet in the case of images [17, 56, 60, 88, 95]. Several methods have been developed to pre-train on complex 3D indoor and outdoor scenes [53, 74, 81, 87]. Inspired by their vision counterpart, these methods also mainly use contrastive and reconstruction objectives. Some works leverage LiDAR specific augmentations [43] or use specialized tasks such as occupancy prediction consistent under sparse point sampling [1, 8] and different mixing strategies for pointclouds [42, 52, 79]. However, these methods are limited by the volume of diverse 3D pre-training data, owing to the difficulty in collecting such a large-scale dataset.

**Cross-modal 2D-to-3D Knowledge Distillation:** Recently, distilling knowledge from a pre-trained 2D image backbone (usually a VFM such as DINOv2 [54]) into a 3D LiDAR backbone has been shown to be an effective pre-training strategy. Initial works focused on single object pointclouds [22, 91] but recent works have demonstrated that this strategy is also suitable for complex scenes [48, 50]. SLidR [61] groups points and pixels into semantically coherent superpixels/superpoints based on the teacher vision model features. Other works use additional vision models such as SAM [37] or OpenSeeD [90] to extract pseudo-semantics regions for the same purpose [49, 83]. Recently, some works have also used spatial and

temporal consistency to regularize learned representations [49, 83, 84, 93, 94]. Recently, ScaLR [57] demonstrated the potential of scaling up different distillation components such as the dataset, the 3D backbone and the 2D backbone while using a simple distillation loss that matches the corresponding point-pixel features directly. However, direct feature comparison impairs the 3D network’s ability to learn geometrically rich features. In this work, we propose an MLP projection head and the auxiliary spatial task of occupancy prediction, to guide the 3D network towards learning more spatially aware features.

### 3. Method Description

In the following, we introduce our considered problem setting as well as our **CleverDistiller** framework shown in Fig. 2.

#### 3.1. Problem Definition and Motivation

Given a point cloud  $\mathcal{P} = \{\mathbf{p}_i \mid i = 1, \dots, N\}$  with  $N$  points captured by a LiDAR sensor, where  $\mathbf{p}_i \in \mathbb{R}^4$  denotes the coordinates of the point and the laser intensity. Let  $\mathcal{I}_t = \{\mathbf{I}_k \mid k = 1, \dots, M\}$  denote  $M$  surround camera images where  $\mathbf{I}_k \in \mathbb{R}^{H \times W \times 3}$  denotes an image with height  $H$  and width  $W$ . The objective of cross-modal distillation is to take advantage of a pre-trained vision foundation model  $T_\phi(\cdot)$  to learn a LiDAR foundation model,  $S_{\theta_p}(\cdot)$  by distilling the features from the image modality to the LiDAR modality.

Many recent works generate a set of class-agnostic or pseudo-semantic superpixels for each image using additional supervised or unsupervised segmentation and clustering models such as SAM [37] or OpenSeeD [90]. This introduces the implicit assumption of feature regularity within each mask or superpixel. Also, these masks and superpixels are not ground truths and require careful hyperparameter tuning to obtain suitable segments for a particular domain. This complicates the overall distillation process and we question the need for semantic priors in the presence of good features from a VFM.

Further, most of the previous works use a contrastive loss [49, 83, 84, 92, 93] which may create an unnecessary *self-conflict* issue. Specifically, in our approach we find corresponding point and image features, without relying on any additional processing steps or semantic priors. Assuming that the point cloud  $\mathcal{P}_t$  and images  $\mathcal{I}_t$  are calibrated, we find corresponding points and pixels by projecting the point cloud  $\mathbf{p}_i = (x_i, y_i, z_i)$  onto the image plane  $(u_i, v_i)$  using the following sensor calibration parameters:

$$\begin{bmatrix} u_i \\ v_i \\ 1 \end{bmatrix} = \rho(i) = \frac{1}{z_i} \times \Gamma_K \times \Gamma_{c \leftarrow l} \times \begin{bmatrix} x_i \\ y_i \\ z_i \end{bmatrix},$$

where  $\Gamma_K$  denotes the camera-intrinsic matrix and  $\Gamma_{c \leftarrow l}$  is the transformation matrix from LiDAR sensors to

surround-view cameras. This enables a direct mapping between points and pixels in the image.

#### 3.2. Cross-modal Learning Objectives

Let the student model,  $S_{\theta_p} : \mathbb{R}^{N \times 4} \rightarrow \mathbb{R}^{N \times D_p}$  be a 3D backbone with trainable parameters  $\theta_p$ , which takes LiDAR points as input and outputs  $D$ -dimensional point features. Let  $T_\phi : \mathbb{R}^{H \times W \times 3} \rightarrow \mathbb{R}^{\frac{H}{S} \times \frac{W}{S} \times D_v}$  be an image backbone with pre-trained parameters  $\phi$  that takes images as input and outputs  $D_v$ -dimensional image features.

The objective function for such a self-supervised knowledge distillation is formulated as,  $\mathcal{L}_{\text{distillation}}(\mathbf{q}_p, \mathbf{q}_v)$ , where the primary objective is to transfer knowledge from the trained image backbone  $T_\phi$  to the 3D backbone  $S_{\theta_p}$ . The point features are obtained as  $\mathbf{q}_p = \mathcal{H}_p(S_{\theta_p}(\mathbf{p}))$  and image features  $\mathbf{q}_v = T_\phi(\mathbf{I})$ , where  $\mathcal{H}_p : \mathbb{R}^{D_p} \rightarrow \mathbb{R}^{D_v}$  is a projection head that transforms the point features to the same dimensions as the VFM teacher. Inspired by ScaLR [57], we use a simple pointwise cosine similarity loss given by,

$$\mathcal{L}_{\text{distillation}}(\mathbf{q}_p, \mathbf{q}_v) = \frac{1}{N} \sum_{i \in \{1, \dots, N\}} \|\mathbf{q}_{p,i} - \mathbf{q}_{v,\rho(i)}\|_2. \quad (1)$$

Such a loss is preferable to a contrastive loss as it avoids the complexities of careful negative sample selection, training sensitivity to batch composition and self-conflict issues while maintaining robust feature alignment.

#### 3.3. Improving the Projection Head

Despite demonstrating that a simple approach can work for distillation, ScaLR yields subpar results compared to methods incorporating additional models, processing steps, or semantic priors [49, 83]. We found that while leveraging ScaLR approach can be beneficial, improving the projection head, a component overlooked in prior works, can significantly improve knowledge transfer.

We investigate the role of the projection head by evaluating the informativeness of the 3D backbone features using the RankMe metric [27]. The RankMe metric has been shown to be indicative of the informativeness of the learned representations and the downstream performance of self-supervised models. We find this to be valid for distillation features as well - features with a higher RankMe metric produce better downstream performance (see Fig. 3). ScaLR uses a linear 3D projection head and we discover that this results in less informative 3D backbone features (see Tab. 1). Using an MLP projection head improves the informativeness of the 3D backbone features as evidenced by the improved RankMe metric. Consequently, this results in significant downstream performance improvements (see Tab. 1). A deeper MLP with larger hidden dimensions results in the most informative backbone features and best downstream performance. A complex MLP projection head

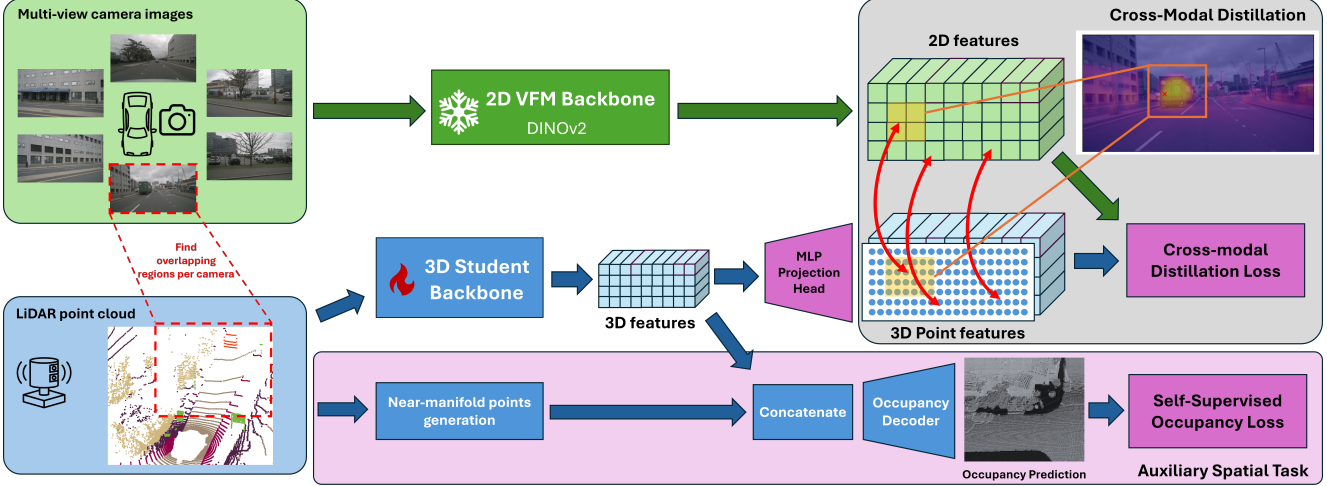


Figure 2. Overview of the **CleverDistiller** framework. First, corresponding points and camera regions are identified based on sensor calibration data. Next, features from cameras and points are extracted using their respective backbones. Two tasks are employed for representation learning: First, the cross-modal KD loss is applied to distill features from the camera to the 3D backbone with our novel MLP projection head allowing the 3D network to learn complex semantics throughout the projection. Second, we employ an occupancy loss to learn spatially consistent feature representation. After pre-training, the 3D backbone can be utilized for various downstream tasks.

adds only a minimal increase in computational cost. Based on this analysis, we use a 3-layer MLP projection head with a similar formulation as the MLP head used while pre-training the DINOv2 model. Following these experiments, we set for using MLP projection head with 3 layers and 2048 hidden dim, that (as shown in Tab. 1 and Fig. 3) yields the best results and retain the most informativeness without significant increase computational cost or memory.

### 3.4. Auxiliary Spatial Occupancy Task

Cross-modal distillation alone is insufficient for optimal performance as it ignores the rich spatial information unique to LiDAR that can be useful for downstream tasks. To enhance the LiDAR model’s spatial understanding and to encourage the learning of LiDAR specific features, we incorporate an auxiliary spatial task. While many works prioritize segmentation tasks where semantic knowledge is dominant, tasks such as 3D object detection (3DOD) require a deeper comprehension of spatial relationships. We experimented with auxiliary tasks like scene flow estimation and occupancy prediction, ultimately selecting occupancy as the most effective. Additionally, while previous works, such as SuperFlow [83], claim to enforce temporal consistency, our analysis revealed that their approach relies on semantic consistency (regions are matched based on the OpenSeeD class vocabulary rather than scene flow) across frames rather than on true temporal feature alignment.

We incorporate an auxiliary spatial understanding task, specifically, occupancy prediction. This injects spatial and geometric information of the objects into the learned features, which we expect to be useful for tasks such as 3D object detection. The occupancy prediction loss is formulated

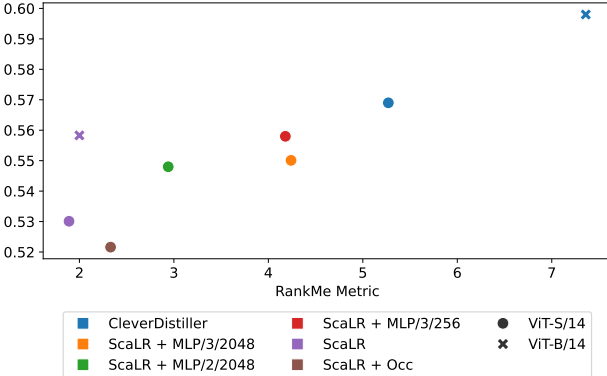


Figure 3. Analysis of 1% finetuning MinkUnet [19] performance on nuScenes dataset (mIoU) vs RankMe metric of the 3D backbone features. We observe clear correlation between RankMe metric and 3D segmentation performance. The colors refers to the used distillation setup, ● are using ViT-S/14 as a teacher and × ViT-B/14.

MLP Layers.	Hidden dim.	RankMe	nuScenes		KITTI		Waymo	
			LP	1%	1%	1%	1%	1%
1 (Linear)	-	1.89	40.76	53.01	44.42	47.98		
2	2048	2.94	45.46	54.38	50.09	48.19		
3	256	4.18	44.79	54.80	50.10	48.93		
3	2048	<b>4.24</b>	<b>46.36</b>	<b>55.01</b>	<b>50.15</b>	<b>49.08</b>		

Table 1. Comparison of different MLP architectures with the PT-v3 [75] 3D backbone model. The MLP projection improves performance as well as the RankMe metric. All scores in mIoU.

based on ALSO [8]. We observe that incorporating the occupancy task improves the informativeness of the backbone features by enabling it to learn additional information complementary to those distilled from the VFM features (see improvement on RankMe metric when adding the occupancy task in Tab. 3). We find that this further boosts downstream performance in various tasks. The effective semantic information from the 2D backbone combined with the spatial knowledge encouraged by this task enable the model to understand and interpret complex 3D environments better. This also makes the model more robust to domain shifts and LiDAR corruption.

Following ALSO [8], for each 3D point  $p$  sampled on the surface, we create two query points:  $q_{\text{front}} = p - \delta p$  and  $q_{\text{behind}} = p + \delta p$ , where  $\delta p$  is a small distance. We consider  $q_{\text{front}}$  to be empty and  $q_{\text{behind}}$  to be filled. Additionally, a third empty query point  $q_{\text{sight}}$  is randomly picked in the segment between the sensor and  $p$ . An occupancy decoder head takes a concatenation of the 3D backbone features and the 3D coordinates of the associated point to predict the occupancy of that point and the intensity of that point. The occupancy loss consists of a binary cross-entropy loss  $\mathcal{L}_{\text{O}}$  based on the occupancy classification and a reconstruction MSE loss  $\mathcal{L}_{\text{Int}}$  based on the intensity prediction and use  $\lambda = 1$  similar to ALSO:

$$\mathcal{L}_{\text{occ}} = \mathcal{L}_{\text{O}} + \lambda \mathcal{L}_{\text{Int}} \quad (2)$$

Overall, we combine two simple but significant design choices. First, we use an MLP projection head and cosine similarity loss. Second, we add a complementary auxiliary spatial task. Combined, these improve the informativeness and spatial consistency of the 3D backbone features as well as downstream performance. This combination of design choices leads to a more robust and efficient cross-modal distillation framework.

## 4. Results

### 4.1. Experiments setup

**Implementation:** CleverDistiller is implemented using the Pointcept [20] codebase. Consistent with prior works we employ MinkUNet [19] as the 3D backbone and DINov2 [54] (with ViT backbones [23]) as the 2D backbone, distilling from three variants: small (S), base (B) and large (L). Additionally, we experiment with a more flexible SOTA 3D backbone, PointTransformer-V3 (PT-v3) [75], to investigate if our method scales to larger models. For PT-v3, we use the default configuration and only increase the decoder dimensions to 256. The framework is pre-trained end-to-end on nuScenes using 4 GPUs for 50 and 100 epochs. We follow the same procedure to pre-train the baseline ScaLR model. We trained our model and ScaLR (official ScaLR results on MinkUnet are very limited [57]), while other results

are based on what authors reported [49, 51, 61, 83, 84].

The distilled LiDAR backbone is then evaluated on a range of downstream tasks on various datasets. Firstly, we conduct segmentation experiments on nuScenes using linear probing and limited data finetuning scenarios using 4 GPUs for 100 epochs, utilizing the AdamW optimizer and OneCycle scheduler. The domain generalization study using Robo3D adheres to the same protocol as previous works. We also test our features for the 3D object detection (3DOD) task on the KITTI and Waymo datasets. For 3DOD, we use weights obtained during pre-training on nuScenes. We substitute PointRCNN [62] backbone (PointNet) with MinkUNet backbone (following SLiDR approach). Finally, we train for 80 epochs on partial data on Waymo and Kitti datasets. Our framework can also work with any other point-based 3D backbone.

Though most cross-modal image-to-LiDAR distillation works claim to pre-train for only 50 epochs, some recent works such as SuperFlow [83] utilize 3 LiDAR sweeps per sample, increasing the effective length and compute cost of the training by a factor of three (effectively 150 epochs). We characterize this using effective epochs in Tab. 4. For fairer comparison, we show results of our method for both 50 and 100 epochs of pre-training. CleverDistiller<sup>50</sup> provides a direct comparison to previous methods that used only one LiDAR sweep per sample while CleverDistiller<sup>100</sup> serves as a more efficient comparison to Superflow. After pre-training we fine-tune the models for 100 epochs.

We experiment on a total of nine datasets in our experiments, namely: nuScenes [9], SemanticKITTI [7] (SKITTI), KITTI [28], Waymo [64], ScribbleKITTI [69], RELLIS-3D [35], SemanticSTF [80], and DAPS-3D [39] and nuscenes-C from Robo3D [40].

**Evaluation Protocols:** Following standard conventions, we report the Intersection-over-Union (IoU) on each semantic class and mean IoU (mIoU) over all classes for downstream tasks. For 3D robustness evaluations, we follow Robo3D [40] and report the mean Corruption Error (mCE) and mean Resilience Rate (mRR). Evaluations are without test-time augmentations.

Occupancy loss weight	nuScenes		SKITTI	Waymo
	LP	1%	1%	1%
0.0	55.72	61.79	56.30	60.78
0.01	56.49	61.40	57.01	62.14
0.05	<b>58.49</b>	<b>62.54</b>	<b>62.19</b>	61.95
0.2	57.39	61.65	58.96	<b>62.39</b>
1.0	53.89	58.99	56.78	62.30

Table 2. Comparison of different occupancy loss weights. All results in mIoU.

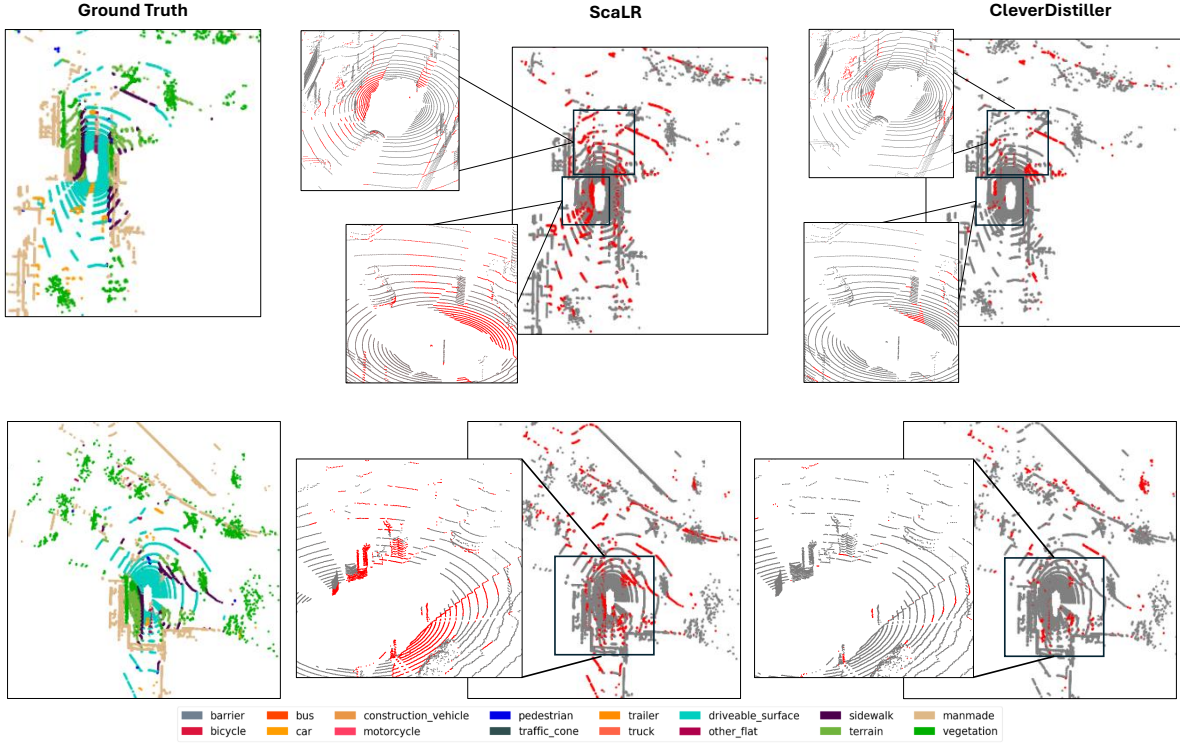


Figure 4. Qualitative segmentation results comparing our CleverDistiller (right) to ScaLR (middle) and the ground truth (left). Legend corresponds to the ground truth. For ScaLR [57] and CleverDistiller we show prediction errors (in red), showcasing that our approach exhibits much less errors. Each row is a different sequence randomly sampled from nuScenes [9].

## 4.2. Ablation studies

We conduct ablation studies for the two components that we added: the MLP projection head and the auxiliary occupancy task. We pre-train a MinkUNet-34 model for 100 epochs using the ViT-S/14 variant of DINOv2. We use the 3-layer MLP head selected in Sec. 3.3 and experimented with different weights for the occupancy loss. From Tab. 2, we see that a weight of 0.05 is sufficient to incorporate additional spatial information. Then, we ablate the best versions of the two components Tab. 3. We observe that the addition of the MLP (c) improves the informativeness of the backbone features and provides a significant performance boost compared to the baseline (a) in Tab. 3. The occupancy task

provides an orthogonal improvement that further improves the backbone features.

## 4.3. Performance Comparison

Leveraging data representation learning can significantly reduce the dependency on data annotations. We evaluate CleverDistiller against prior SOTA methods on three prominent datasets: nuScenes, SemanticKITTI, and Waymo, under scenarios with limited annotations for few-shot fine-tuning. As illustrated in Tab. 4 and Tab. 5, CleverDistiller demonstrates SOTA performance across all fine-tuning tasks as well as on linear probing on almost every scenario on both MinkUnet [19] and PTV3 [75]. Especially when fine-tuning on low data amounts on nuScenes we observe strong improvements of up to 10% mIoU, e.g. for 1% nuScenes data and ViT-L DINOv2 teacher. This performance indicates strong generalization of our learned feature representations, making our work highly relevant for use cases with low data availability. The tables also show that models pretrained through representation learning consistently surpass those initialized randomly, highlighting the benefits of data pretraining. Additionally, distillations from larger 2D networks yield consistent enhancements which is consistent with observations in previous works.

We can also observe in Fig. 4 that our predictions have

#	MLP	Occ	Matrix Rank	RankMe	nuScenes		SKITTI		Waymo	
					LP	1%	1%	1%	1%	1%
(a)	<span style="color: red;">✗</span>	<span style="color: red;">✗</span>	22	1.89	40.76	53.01	44.42	47.98		
(b)	<span style="color: red;">✗</span>	<span style="color: green;">✓</span>	25	2.33	41.67	52.16	48.19	48.11		
(c)	<span style="color: green;">✓</span>	<span style="color: red;">✗</span>	33	4.24	46.36	55.01	50.15	49.08		
(d)	<span style="color: green;">✓</span>	<span style="color: green;">✓</span>	41	5.27	49.81	56.90	50.59	50.99		

Table 3. Ablation study of our components, showing the effectiveness of both the MLP projection head and the auxiliary occupancy task (Occ) individually. All results in mIoU.

Method	Venue	Distill	Semantic Priors	Effective Epochs	nuScenes							SKITTI	Waymo
					LP	1%	5%	10%	25%	Full	1%		
Random	-	-	✗	-	8.10	30.30	47.84	56.15	65.48	74.66	39.50	39.41	
PPKT [51]	arXiv'21	ViT-S	✗	50	38.60	40.60	52.06	59.99	65.76	73.97	43.25	47.44	
SLidR [61]	CVPR'22	ViT-S	✓	50	44.70	41.16	53.65	61.47	66.71	74.20	44.67	47.57	
Seal [49]	NeurIPS'23	ViT-S	✓	50	45.16	44.27	55.13	62.46	67.64	75.58	46.51	48.67	
CleverDistiller <sup>50</sup>	-	ViT-S	✗	50	<b>46.02</b>	<b>53.67</b>	<b>62.34</b>	<b>64.04</b>	<b>68.06</b>	<b>77.44</b>	<b>49.58</b>	<b>50.45</b>	
SuperFlow [83]	ECCV'24	ViT-S	✓	150	46.44	47.81	59.44	64.47	69.20	76.54	47.97	49.94	
ScalLR [57]	CVPR'24	ViT-S	✗	100	40.76	53.01	61.58	63.47	67.56	74.51	44.42	47.98	
LiMoE [84]	CVPR'25	ViT-S	✓	150	48.20	49.60	60.54	65.65	<b>71.39</b>	77.27	49.53	<b>51.42</b>	
CleverDistiller <sup>100</sup>	-	ViT-S	✗	100	<b>49.81</b>	<b>56.90</b>	<b>64.55</b>	<b>65.92</b>	70.11	<b>77.61</b>	<b>50.59</b>	50.99	
PPKT [51]	arXiv'21	ViT-B	✗	50	39.95	40.91	53.21	60.87	66.22	74.07	44.09	47.57	
SLidR [61]	CVPR'22	ViT-B	✓	50	45.35	41.64	55.83	62.68	67.61	74.98	45.50	48.32	
Seal [49]	NeurIPS'23	ViT-B	✓	50	46.59	45.98	57.15	62.79	68.18	75.41	47.24	48.91	
CleverDistiller <sup>50</sup>	-	ViT-B	✗	50	<b>48.40</b>	<b>55.80</b>	<b>63.49</b>	<b>65.56</b>	<b>69.06</b>	<b>78.17</b>	<b>49.83</b>	<b>52.80</b>	
SuperFlow [83]	ECCV'24	ViT-B	✓	150	47.66	48.09	59.66	64.52	69.79	76.57	48.40	50.20	
ScalLR [57]	CVPR'24	ViT-B	✗	100	41.80	55.83	63.46	65.24	68.70	74.76	45.59	49.60	
LiMoE [84]	CVPR'25	ViT-B	✓	150	49.07	50.23	61.51	66.17	<b>71.56</b>	77.81	50.30	51.77	
CleverDistiller <sup>100</sup>	-	ViT-B	✗	100	<b>51.89</b>	<b>59.80</b>	<b>66.44</b>	<b>67.65</b>	69.53	<b>78.49</b>	<b>51.48</b>	<b>53.56</b>	
PPKT [51]	arXiv'21	ViT-L	✗	50	41.57	42.05	55.75	61.26	66.88	74.33	45.87	47.82	
SLidR [61]	CVPR'22	ViT-L	✓	50	45.70	42.77	57.45	63.20	68.13	75.51	47.01	48.60	
Seal [49]	NeurIPS'23	ViT-L	✓	50	46.81	46.27	58.14	63.27	68.67	75.66	47.55	50.02	
CleverDistiller <sup>50</sup>	-	ViT-L	✗	50	<b>48.32</b>	<b>56.70</b>	<b>64.51</b>	<b>66.25</b>	<b>69.33</b>	<b>78.68</b>	<b>49.86</b>	<b>53.32</b>	
SuperFlow [83]	ECCV'24	ViT-L	✓	150	48.01	49.95	60.72	65.09	70.01	77.19	49.07	50.67	
ScalLR [57]	CVPR'24	ViT-L	✗	100	40.12	55.78	63.28	64.76	68.19	75.09	44.85	50.34	
LiMoE [84]	CVPR'25	ViT-L	✓	150	49.35	51.41	62.07	66.64	<b>71.59</b>	77.85	50.69	51.93	
CleverDistiller <sup>100</sup>	-	ViT-L	✗	100	<b>52.45</b>	<b>60.64</b>	<b>67.03</b>	<b>67.29</b>	70.45	<b>78.29</b>	<b>52.28</b>	<b>54.83</b>	

Table 4. Comparison of SOTA pretraining methods pretrained in self-supervised manner on nuScenes and fine-tuned on nuScenes, SemanticKITTI, and Waymo. All methods use MinkUNet-34 [19] as the backbone for the 3D semantic segmentation task. We also show which 2D VFM backbone was used as a teacher and if the approach uses pseudo semantic priors from off-the shelf segmentation models. LP denotes linear probing with a frozen backbone. All scores in mIoU. For LiMoE [84], we use LiMoE+Superflow.

Method	Distill	nuScenes					SKITTI	Waymo
		LP	1%	5%	10%	25%	1%	1%
ScalLR [57]	ViT-S	44.99	62.07	69.10	72.91	75.69	56.92	60.09
CleverDistiller	ViT-S	<b>58.49</b>	<b>62.54</b>	<b>71.09</b>	<b>73.89</b>	<b>76.64</b>	<b>61.95</b>	<b>62.19</b>
ScalLR [57]	ViT-B	41.62	63.54	71.74	73.84	76.56	60.74	57.17
CleverDistiller	ViT-B	<b>60.54</b>	<b>63.93</b>	<b>72.27</b>	<b>74.11</b>	<b>76.93</b>	<b>63.31</b>	<b>62.20</b>
ScalLR [57]	ViT-L	45.54	66.17	72.34	74.96	77.56	58.48	61.47
CleverDistiller	ViT-L	<b>61.92</b>	<b>66.18</b>	<b>73.13</b>	<b>75.18</b>	<b>77.57</b>	<b>62.23</b>	<b>65.94</b>

Table 5. Comparisons of state-of-the-art pretraining methods pretrained on nuScenes and fine-tuned on SemanticKITTI and Waymo with specified data portions using PointTransformerV3 [76] as the 3D semantic segmentation backbone. LP denotes linear probing with a frozen backbone. All scores in mIoU.

fewer errors along the segmentation boundaries than those from ScalLR. Types of segmentation errors are not reflected by mIoU scores, but well-defined boundaries are crucial for the output quality. We provide additional qualitative of features and class-specific analysis in supplementary Sec. A2 and Sec. A3.

#### 4.4. Domain generalization

We test our method, pre-trained on nuScenes, on the ScriKITTI, Rellis-3D, SemSTF, and DAPS-3D datasets to show its domain generalization capabilities, as shown

Method	ScriKITTI		Rellis-3D		SemSTF		DAPS-3D	
	1%	10%	1%	10%	50%	100%	50%	100%
Random	23.81	47.60	38.46	53.60	48.03	48.15	74.32	79.38
PPKT <sup>50</sup>	36.50	51.67	49.71	54.33	50.92	54.69	78.90	84.00
SLidR <sup>50</sup>	39.60	50.45	49.75	54.57	52.01	54.35	81.00	85.40
Seal <sup>50</sup>	40.64	52.77	51.09	55.03	53.46	<b>55.36</b>	81.88	85.90
Ours <sup>50</sup>	<b>40.77</b>	<b>53.31</b>	<b>56.23</b>	<b>56.60</b>	<b>53.77</b>	54.72	<b>82.58</b>	<b>86.15</b>
ScalLR <sup>100</sup>	36.45	49.16	47.91	48.86	52.10	54.40	-	-
SF <sup>150</sup>	42.70	54.00	52.83	55.71	54.72	56.57	82.43	86.21
LiMoE <sup>150</sup>	43.95	55.96	53.74	56.67	<b>55.60</b>	<b>57.31</b>	83.24	86.68
Ours <sup>100</sup>	<b>44.03</b>	<b>56.70</b>	<b>58.35</b>	<b>60.92</b>	53.99	55.66	<b>83.06</b>	<b>87.95</b>

Table 6. Domain generalization study of various pretraining methods on the nuScenes, followed by fine-tuning on different 3D semantic segmentation datasets with specified data portions. All scores in mIoU.

in Tab. 6. Each dataset presents unique challenges, and our method consistently performs well. Our approach consistently achieved the highest scores in most cases compared to other SOTA pretraining methods. For instance, on the ScriKITTI dataset, our method reached 40.77 mIoU with 1% data and 53.31 with 10% data, outperforming all other methods. Similarly, on the Rellis-3D dataset, our method achieved 56.23 mIoU with 1% data and 56.60 with 10% data, again leading the performance charts. Even on the

	Method	Backbone	mCE ↓	mRR ↑	mIoU ↑								
					Fog	Rain	Snow	Blur	Beam	Cross	Echo	Sensor	Avg Full
Full	Random	MinkU-34	112.20	72.57	62.96	70.65	55.48	51.71	62.01	31.56	59.64	39.41	54.18
	PPKT <sup>50</sup> [51]	MinkU-34	105.64	75.87	64.01	72.18	59.08	57.17	63.88	36.34	60.59	39.57	56.60
	SLidR <sup>50</sup> [61]	MinkU-34	106.08	75.99	65.41	72.31	56.01	56.07	62.87	41.94	61.16	38.90	56.83
	Seal <sup>50</sup> [49]	MinkU-34	<b>92.63</b>	83.08	72.66	<b>74.31</b>	66.22	<b>66.14</b>	<b>65.96</b>	57.44	59.87	39.85	62.81
	<b>CleverDistiller</b> <sup>50</sup>	MinkU-34	94.90	<b>84.12</b>	<b>72.73</b>	73.33	<b>67.35</b>	56.42	64.14	<b>63.76</b>	<b>60.65</b>	<b>47.27</b>	<b>63.21</b>
	SuperFlow <sup>150</sup> [83]	MinkU-34	91.67	83.17	70.32	75.77	65.41	61.05	68.09	60.02	58.36	50.41	63.68
	Scalr <sup>100</sup> [57]	MinkU-34	99.86	81.35	69.23	72.47	60.67	55.11	64.07	56.93	60.34	46.11	60.62
LP	LiMoE <sup>150</sup>	MinkU-34	<b>88.43</b>	83.28	71.10	<b>75.92</b>	65.66	<b>63.86</b>	<b>68.52</b>	60.78	<b>61.91</b>	50.66	64.80
	<b>CleverDistiller</b> <sup>100</sup>	MinkU-34	91.28	<b>87.42</b>	<b>72.83</b>	70.91	<b>66.03</b>	60.18	66.85	<b>68.04</b>	60.17	<b>53.63</b>	<b>64.83</b>
	PPKT <sup>50</sup> [51]	MinkU-34	183.44	78.15	30.65	35.42	28.12	29.21	32.82	19.52	28.01	20.71	28.06
	SLidR <sup>50</sup> [61]	MinkU-34	179.38	77.18	34.88	38.09	32.64	26.44	33.73	20.81	31.54	21.44	29.95
	Seal <sup>50</sup> [49]	MinkU-34	166.18	75.38	37.33	42.77	29.93	37.73	40.32	20.31	37.73	24.94	33.88
	<b>CleverDistiller</b> <sup>50</sup>	MinkU-34	<b>157.50</b>	<b>84.84</b>	<b>42.45</b>	<b>43.45</b>	<b>38.77</b>	<b>37.85</b>	<b>41.01</b>	<b>43.11</b>	<b>39.17</b>	<b>26.55</b>	<b>39.05</b>
	SuperFlow <sup>150</sup> [83]	MinkU-34	161.78	75.52	37.59	43.42	37.60	39.57	41.40	23.64	38.03	26.69	35.99
LP	Scalr <sup>100</sup> [57]	MinkU-34	173.18	78.91	37.55	37.96	36.29	33.64	33.06	23.01	33.62	23.70	33.59
	LiMoE <sup>150</sup>	MinkU-34	155.77	78.23	40.35	45.28	39.14	<b>42.10</b>	<b>44.21</b>	27.33	39.20	<b>29.49</b>	38.39
	<b>CleverDistiller</b> <sup>100</sup>	MinkU-34	<b>151.21</b>	<b>89.99</b>	<b>43.96</b>	<b>46.91</b>	<b>41.20</b>	41.05	42.15	<b>45.67</b>	<b>41.30</b>	28.85	<b>41.39</b>

Table 7. 3D robustness study of state-of-the-art pretraining methods under corruption and sensor failure scenarios in the nuScenes-C dataset from the Robo3D benchmark [40]. Full denotes fine-tuning with 100% labeled data. LP denotes linear probing with a frozen backbone. All mCE (↓), mRR (↑), and mIoU (↑) scores are given in percentage (%). Best scores in each configuration are shaded with colors.

SemSTF and DAPS-3D datasets, our method demonstrated strong results, particularly excelling with 82.58 mIoU at 50% data and 86.15 at 100% data on DAPS-3D. These results underscore the robustness and generalization of our approach in 3D semantic segmentation tasks.

#### 4.5. Robustness

The robustness of 3D perception models against unprecedented conditions directly correlates with the model’s applicability to real-world applications. We compare our method with prior models in the nuScenes-C dataset from the Robo3D [40] benchmark and show results in Tab. 7. Our method demonstrates superior performance, particularly in corrupted scenarios where other methods struggle, such as when the LiDAR data is much sparser.

CleverDistiller shows improved robustness over random initialization and other methods, achieving the lowest mean Corruption Error (mCE) for linear probing and nearly the lowest for full pre-training. Additionally, our method achieves the highest mean relative robustness (mRR) in all trials, indicating strong resistance to corruptions. For example, in the Fog scenario, our method achieves an mIoU of 72.83, compared to 62.96 for random initialization. The most notable result is in the *Cross* corruption scenario, which involves sparse LiDAR data. While other methods experience a performance drop of approximately 50% on LP and 10-20% on full, CleverDistiller maintains high per-

Method	KITTI			Waymo		
	5%	10%	20%	5%	10%	20%
Random init.	56.1	59.1	61.6	18.0	21.9	28.5
PPKT <sup>50</sup>	57.8	60.1	61.2	-	-	-
SLidR <sup>50</sup>	57.8	61.4	62.4	-	-	-
<b>CleverDistiller</b> <sup>50</sup>	<b>58.3</b>	<b>63.7</b>	<b>66.8</b>	<b>22.7</b>	<b>24.6</b>	<b>26.4</b>
Scalr <sup>100</sup>	56.2	62.3	66.5	20.1	28.1	28.2
<b>CleverDistiller</b> <sup>100</sup>	<b>59.8</b>	<b>66.6</b>	<b>67.1</b>	<b>22.2</b>	<b>28.7</b>	<b>29.6</b>

Table 8. Evaluation of our pre-training approach on 3D object detection benchmarks. All results in mAP.

formance, showcasing its adaptability to sparse data.

#### 4.6. 3D Object Detection

For 3DOD, we use the same features distilled in SSL as we do for segmentation. This means we have one model, one distillation run, and the same features for multiple tasks, ensuring efficiency and consistency. 3D backbone is pre-trained in an unsupervised manner and then used as a backbone in the 3DOD task. Unlike other methods such as Olivine [92] and CMCR [93], which need to distill features to a different network architecture like VoxelNet, our approach uses MinkUNet, making the features useful for both segmentation and 3DOD tasks. In our experiments shown in Tab. 8, we benchmarked our method on the KITTI and Waymo datasets. Our method consistently outperformed

the previous best method by approximately 5-10%, showing that the features are versatile and effective across multiple tasks.

## 5. Conclusions

We introduce CleverDistiller, a framework for cross-modal distillation that achieves SOTA performance using simple and spatially consistent cross-modal distillation. We show that the projection head design plays a crucial role in improving informativeness of the learned representations. Crucially, we observe that our MLP projection head enables better semantic information flow from the 2D VFM model to the 3D backbone. Incorporating an auxiliary spatial tasks, such as occupancy prediction, provides additional supervision signals that enhance the spatial reasoning of the model. The results, both qualitative and quantitative, demonstrate that the learned features are an excellent basis for various downstream tasks, especially in sparse data scenarios where we see improvements by up to 10% mIoU. Since our proposed improvements are widely applicable to other architectures we believe that our contributions will have a high adoption rate by future work on cross-modal knowledge distillation.

## References

- [1] Ben Agro, Quinlan Sykora, Sergio Casas, Thomas Gilles, and Raquel Urtasun. Uno: Unsupervised occupancy fields for perception and forecasting. In *Proceedings of the IEEE/CVF Conference on Computer Vision and Pattern Recognition*, 2024. [2](#)
- [2] Woo-Jin Ahn, Geun-Yeong Yang, Hyun-Duck Choi, and Myo-Taeg Lim. Style blind domain generalized semantic segmentation via covariance alignment and semantic consistency contrastive learning. *Proceedings of the IEEE/CVF Conference on Computer Vision and Pattern Recognition*, 2024. [1](#)
- [3] Yuki Markus Asano, Christian Rupprecht, and Andrea Vedaldi. Self-labelling via simultaneous clustering and representation learning. In *ICLR*, 2020. [2](#)
- [4] Mahmoud Assran, Mathilde Caron, Ishan Misra, Piotr Bojanowski, Florian Bordes, Pascal Vincent, Armand Joulin, Mike Rabbat, and Nicolas Ballas. Masked siamese networks for label-efficient learning. In *ECCV*, 2022. [2](#)
- [5] Randall Balestriero and Yann LeCun. How learning by reconstruction produces uninformative features for perception. In *International Conference on Machine Learning*, 2024. [2](#)
- [6] Hangbo Bao, Li Dong, Songhao Piao, and Furu Wei. BEiT: BERT pre-training of image transformers. In *ICLR*, 2022. [2](#)
- [7] Jens Behley, Martin Garbade, Andres Milioto, Jan Quenzel, Sven Behnke, Cyrill Stachniss, and Jürgen Gall. Semantickitti: A dataset for semantic scene understanding of lidar sequences. In *Proceedings of the IEEE/CVF international conference on computer vision*, pages 9297–9307, 2019. [5](#)
- [8] Alexandre Boulch, Corentin Sautier, Björn Michele, Gilles Puy, and Renaud Marlet. Also: Automotive lidar self-supervision by occupancy estimation. In *Proceedings of the IEEE/CVF Conference on Computer Vision and Pattern Recognition*, 2023. [2, 5](#)
- [9] Holger Caesar, Varun Bankiti, Alex H Lang, Sourabh Vora, Venice Erin Liang, Qiang Xu, Anush Krishnan, Yu Pan, Giancarlo Baldan, and Oscar Beijbom. nuscenes: A multi-modal dataset for autonomous driving. In *Proceedings of the IEEE/CVF Conference on Computer Vision and Pattern Recognition*, pages 11621–11631, 2020. [5, 6](#)
- [10] Mathilde Caron, Piotr Bojanowski, Armand Joulin, and Matthijs Douze. Deep clustering for unsupervised learning of visual features. In *ECCV*, 2018. [2](#)
- [11] Mathilde Caron, Ishan Misra, Julien Mairal, Priya Goyal, Piotr Bojanowski, and Armand Joulin. Unsupervised learning of visual features by contrasting cluster assignments. In *NeurIPS*, 2020. [2](#)
- [12] Mathilde Caron, Hugo Touvron, Ishan Misra, Hervé Jégou, Julien Mairal, Piotr Bojanowski, and Armand Joulin. Emerging properties in self-supervised vision transformers. In *Proceedings of the International Conference on Computer Vision*, pages 9650–9660, 2021. [1, 2](#)
- [13] Angel X. Chang, Thomas Funkhouser, Leonidas Guibas, Pat Hanrahan, Qixing Huang, Zimo Li, Silvio Savarese, Manolis Savva, Shuran Song, Hao Su, Jianxiong Xiao, Li Yi, and Fisher Yu. ShapeNet: An Information-Rich 3D Model Repository. Technical Report arXiv:1512.03012 [cs.GR], 2015. [2](#)
- [14] Ting Chen, Simon Kornblith, Mohammad Norouzi, and Geoffrey Hinton. A simple framework for contrastive learning of visual representations. In *ICML*, 2020. [2](#)
- [15] Xinlei Chen, Haoqi Fan, Ross Girshick, and Kaiming He. Improved baselines with momentum contrastive learning. *arXiv preprint arXiv:2003.04297*, 2020. [2](#)
- [16] Xinlei Chen, Saining Xie, and Kaiming He. An empirical study of training self-supervised vision transformers. In *ICCV*, 2021. [2](#)
- [17] Ye Chen, Jinxian Liu, Bingbing Ni, Hang Wang, Jiancheng Yang, Ning Liu, Teng Li, and Qi Tian. Shape self-correction for unsupervised point cloud understanding. In *Proceedings of the International Conference on Computer Vision*, 2021. [2](#)
- [18] Zehui Chen, Zhenyu Li, Shiquan Zhang, Liangji Fang, Qin-hong Jiang, and Feng Zhao. Bevdistill: Cross-modal bev distillation for multi-view 3d object detection. *arXiv preprint arXiv:2211.09386*, 2022. [2](#)
- [19] Christopher Choy, JunYoung Gwak, and Silvio Savarese. 4d spatio-temporal convnets: Minkowski convolutional neural networks. In *Proceedings of the IEEE/CVF Conference on Computer Vision and Pattern Recognition*, pages 3075–3084, 2019. [4, 5, 6, 7](#)
- [20] Pointcept Contributors. Pointcept: A codebase for point cloud perception research. <https://github.com/Pointcept/Pointcept>, 2023. [5](#)
- [21] Jia Deng, Wei Dong, Richard Socher, Li-Jia Li, Kai Li, and Li Fei-Fei. Imagenet: A large-scale hierarchical image database. In *CVPR*, 2009. [2](#)

- [22] Runpei Dong, Zekun Qi, Linfeng Zhang, Junbo Zhang, Jianjian Sun, Zheng Ge, Li Yi, and Kaisheng Ma. Autoencoders as cross-modal teachers: Can pretrained 2d image transformers help 3d representation learning? In *Proceedings of the International Conference on Learning Representations*, 2023. 2
- [23] Alexey Dosovitskiy, Lucas Beyer, Alexander Kolesnikov, Dirk Weissenborn, Xiaohua Zhai, Thomas Unterthiner, Mostafa Dehghani, Matthias Minderer, Georg Heigold, Sylvain Gelly, et al. An image is worth 16x16 words: Transformers for image recognition at scale. In *ICLR*, 2021. 5
- [24] Johan Edstedt, Qiyu Sun, Georg Bökman, Mårten Wadenbäck, and Michael Felsberg. Roma: Robust dense feature matching. In *Proceedings of the IEEE/CVF Conference on Computer Vision and Pattern Recognition*, 2024. 2
- [25] Linus Ericsson, Henry Gouk, and Timothy M Hospedales. How well do self-supervised models transfer? In *CVPR*, 2021. 2
- [26] George Eskandar, Chongzhe Zhang, Abhishek Kaushik, Karim Guirguis, Mohamed Sayed, and Bin Yang. An empirical study of the generalization ability of lidar 3d object detectors to unseen domains. *Proceedings of the IEEE/CVF Conference on Computer Vision and Pattern Recognition*, 2024. 1
- [27] Quentin Garrido, Randall Balestrieri, Laurent Najman, and Yann Lecun. Rankme: Assessing the downstream performance of pretrained self-supervised representations by their rank. In *International Conference on Machine Learning*, 2023. 3
- [28] Andreas Geiger, Philip Lenz, Christoph Stiller, and Raquel Urtasun. Vision meets robotics: The kitti dataset. *The International Journal of Robotics Research*, 2013. 5
- [29] Hariprasath Govindarajan, Per Sidén, Jacob Roll, and Fredrik Lindsten. Dino as a von mises-fisher mixture model. In *Proceedings of the International Conference on Learning Representations*, 2023. 2
- [30] Guangxing Han and Ser-Nam Lim. Few-shot object detection with foundation models. In *Proceedings of the IEEE/CVF Conference on Computer Vision and Pattern Recognition*, 2024. 2
- [31] Kaiming He, Xiangyu Zhang, Shaoqing Ren, and Jian Sun. Deep residual learning for image recognition. In *Proceedings of the IEEE/CVF Conference on Computer Vision and Pattern Recognition*, 2016. 2
- [32] Kaiming He, Haoqi Fan, Yuxin Wu, Saining Xie, and Ross Girshick. Momentum contrast for unsupervised visual representation learning. In *CVPR*, 2020. 2
- [33] Kaiming He, Xinlei Chen, Saining Xie, Yanghao Li, Piotr Dollár, and Ross Girshick. Masked autoencoders are scalable vision learners. In *CVPR*, 2022. 2
- [34] Chengjie Huang, Vahdat Abdelzad, Sean Sedwards, and Krzysztof Czarnecki. Soap: Cross-sensor domain adaptation for 3d object detection using stationary object aggregation pseudo-labelling. In *Proceedings of the IEEE/CVF Winter Conference on Applications of Computer Vision*, pages 3352–3361, 2024. 1
- [35] Peng Jiang, Philip Osteen, Maggie Wigness, and Srikanth Saripalli. Rellis-3d dataset: Data, benchmarks and analysis. In *2021 IEEE international conference on robotics and automation (ICRA)*, pages 1110–1116. IEEE, 2021. 5
- [36] Alexander Kirillov, Eric Mintun, Nikhila Ravi, Hanzi Mao, Chloe Rolland, Laura Gustafson, Tete Xiao, Spencer Whitehead, Alexander C Berg, Wan-Yen Lo, et al. Segment anything. In *Proceedings of the IEEE/CVF international conference on computer vision*, pages 4015–4026, 2023. 1
- [37] Alexander Kirillov, Eric Mintun, Nikhila Ravi, Hanzi Mao, Chloe Rolland, Laura Gustafson, Tete Xiao, Spencer Whitehead, Alexander C Berg, Wan-Yen Lo, et al. Segment anything. In *Proceedings of the International Conference on Computer Vision*, 2023. 2, 3
- [38] Marvin Klingner, Shubhankar Borse, Varun Ravi Kumar, Behnaz Rezaei, Venkatraman Narayanan, Senthil Yogamani, and Fatih Porikli. X3kd: Knowledge distillation across modalities, tasks and stages for multi-camera 3d object detection. In *Proceedings of the IEEE/CVF Conference on Computer Vision and Pattern Recognition*, 2023. 2
- [39] Alexey A Klokov, Di Un Pak, Aleksandr Khorin, Dmitry A Yudin, Leon Kochiev, Vladimir D Luchinskiy, and Vitaly D Bezuglyj. Daps3d: Domain adaptive projective segmentation of 3d lidar point clouds. *IEEE Access*, 11:79341–79356, 2023. 5
- [40] Lingdong Kong, Youquan Liu, Xin Li, Runnan Chen, Wenwei Zhang, Jiawei Ren, Liang Pan, Kai Chen, and Ziwei Liu. Robo3d: Towards robust and reliable 3d perception against corruptions. In *Proceedings of the International Conference on Computer Vision*, pages 19994–20006, 2023. 5, 8
- [41] Lingdong Kong, Niamul Quader, and Venice Erin Liong. Conda: Unsupervised domain adaptation for lidar segmentation via regularized domain concatenation. In *2023 IEEE International Conference on Robotics and Automation (ICRA)*, pages 9338–9345. IEEE, 2023. 1
- [42] Lingdong Kong, Jiawei Ren, Liang Pan, and Ziwei Liu. Lasermix for semi-supervised lidar semantic segmentation. In *Proceedings of the IEEE/CVF Conference on Computer Vision and Pattern Recognition*, pages 21705–21715, 2023. 2
- [43] Lingdong Kong, Xiang Xu, Jiawei Ren, Wenwei Zhang, Liang Pan, Kai Chen, Wei Tsang Ooi, and Ziwei Liu. Multi-modal data-efficient 3d scene understanding for autonomous driving. *IEEE Transactions on Pattern Analysis and Machine Intelligence*, 2025. 2
- [44] Alex Krizhevsky, Ilya Sutskever, and Geoffrey E Hinton. Imagenet classification with deep convolutional neural networks. *NeurIPS*, 2012. 2
- [45] Tim Lebailly, Thomas Stegmüller, Behzad Bozorgtabar, Jean-Philippe Thiran, and Tinne Tuytelaars. Cribo: Self-supervised learning via cross-image object-level bootstrapping. In *Proceedings of the International Conference on Learning Representations*, 2024. 1, 2
- [46] Junnan Li, Pan Zhou, Caiming Xiong, and Steven Hoi. Prototypical contrastive learning of unsupervised representations. In *ICLR*, 2020. 2
- [47] Ziyu Li, Jingming Guo, Tongtong Cao, Liu Bingbing, and Wankou Yang. Gpa-3d: Geometry-aware prototype align-

- ment for unsupervised domain adaptive 3d object detection from point clouds. In *Proceedings of the International Conference on Computer Vision*, pages 6394–6403, 2023. 1
- [48] Youquan Liu, Lingdong Kong, Jun Cen, Runnan Chen, Wen-wei Zhang, Liang Pan, Kai Chen, and Ziwei Liu. Segment any point cloud sequences by distilling vision foundation models. *NeurIPS*, 2023. 2
- [49] Youquan Liu, Lingdong Kong, Jun Cen, Runnan Chen, Wen-wei Zhang, Liang Pan, Kai Chen, and Ziwei Liu. Segment any point cloud sequences by distilling vision foundation models. *Advances in Neural Information Processing Systems*, 36, 2024. 2, 3, 5, 7, 8
- [50] Yueh-Cheng Liu, Yu-Kai Huang, Hung-Yueh Chiang, Hung-Ting Su, Zhe-Yu Liu, Chin-Tang Chen, Ching-Yu Tseng, and Winston H Hsu. Learning from 2d: Contrastive pixel-to-point knowledge transfer for 3d pretraining. *arXiv preprint arXiv:2104.04687*, 2021. 2
- [51] Yueh-Cheng Liu, Yu-Kai Huang, Hung-Yueh Chiang, Hung-Ting Su, Zhe-Yu Liu, Chin-Tang Chen, Ching-Yu Tseng, and Winston H Hsu. Learning from 2d: Contrastive pixel-to-point knowledge transfer for 3d pretraining. *arXiv preprint arXiv:2104.04687*, 2021. 5, 7, 8
- [52] Alexey Nekrasov, Jonas Schult, Or Litany, Bastian Leibe, and Francis Engelmann. Mix3D: Out-of-Context Data Augmentation for 3D Scenes. In *Proceedings of the International Conference on 3D Vision (3DV)*, 2021. 2, 13
- [53] Lucas Nunes, Rodrigo Marcuzzi, Xieyuanli Chen, Jens Behley, and Cyrill Stachniss. Segcontrast: 3d point cloud feature representation learning through self-supervised segment discrimination. *IEEE Robotics and Automation Letters*, 2022. 2
- [54] Maxime Oquab, Timothée Darcet, Théo Moutakanni, Huy Vo, Marc Szafraniec, Vasil Khalidov, Pierre Fernandez, Daniel Haziza, Francisco Massa, Alaaeldin El-Nouby, et al. Dinov2: Learning robust visual features without supervision. *arXiv preprint arXiv:2304.07193*, 2023. 1, 2, 5
- [55] Xidong Peng, Xinge Zhu, and Yuexin Ma. Cl3d: Unsupervised domain adaptation for cross-lidar 3d detection. In *Proceedings of the AAAI Conference on Artificial Intelligence*, pages 2047–2055, 2023. 1
- [56] Omid Poursaeed, Tianxing Jiang, Han Qiao, Nayun Xu, and Vladimir G Kim. Self-supervised learning of point clouds via orientation estimation. In *Proceedings of the International Conference on 3D Vision (3DV)*. IEEE, 2020. 2
- [57] Gilles Puy, Spyros Gidaris, Alexandre Boulch, Oriane Siméoni, Corentin Sautier, Patrick Pérez, Andrei Bursuc, and Renaud Marlet. Three pillars improving vision foundation model distillation for lidar. In *Proceedings of the IEEE/CVF Conference on Computer Vision and Pattern Recognition*, pages 21519–21529, 2024. 2, 3, 5, 6, 7, 8
- [58] Yangjun Ruan, Saurabh Singh, Warren Richard Morningstar, Alexander A Alemi, Sergey Ioffe, Ian Fischer, and Joshua V Dillon. Weighted ensemble self-supervised learning. In *ICLR*, 2023. 2
- [59] Cristiano Saltori, Stephane Lathuiliere, Nicu Sebe, Elisa Ricci, and Fabio Galasso. Sf-uda 3d: Source-free unsupervised domain adaptation for lidar-based 3d object detection. In *Proceedings of the International Conference on 3D Vision (3DV)*, pages 771–780. IEEE, 2020. 1
- [60] Jonathan Sauder and Bjarne Sievers. Self-supervised deep learning on point clouds by reconstructing space. *NeurIPS*, 2019. 2
- [61] Corentin Sautier, Gilles Puy, Spyros Gidaris, Alexandre Boulch, Andrei Bursuc, and Renaud Marlet. Image-to-lidar self-supervised distillation for autonomous driving data. In *Proceedings of the IEEE/CVF Conference on Computer Vision and Pattern Recognition*, pages 9891–9901, 2022. 2, 5, 7, 8
- [62] Shaoshuai Shi, Xiaogang Wang, and Hongsheng Li. Pointrcnn: 3d object proposal generation and detection from point cloud. In *Proceedings of the IEEE/CVF Conference on Computer Vision and Pattern Recognition*, pages 770–779, 2019. 5
- [63] Thomas Stegmüller, Tim Lebailly, Behzad Bozorgtabar, Tinne Tuytelaars, and Jean-Philippe Thiran. Croc: Cross-view online clustering for dense visual representation learning. In *Proceedings of the IEEE/CVF Conference on Computer Vision and Pattern Recognition*, pages 7000–7009, 2023. 1
- [64] Pei Sun, Henrik Kretzschmar, Xerxes Dotiwalla, Aurelien Chouard, Vijaysai Patnaik, Paul Tsui, James Guo, Yin Zhou, Yuning Chai, Benjamin Caine, et al. Scalability in perception for autonomous driving: Waymo open dataset. In *Proceedings of the IEEE/CVF Conference on Computer Vision and Pattern Recognition*, pages 2446–2454, 2020. 5
- [65] Hugo Touvron, Matthieu Cord, Matthijs Douze, Francisco Massa, Alexandre Sablayrolles, and Hervé Jégou. Training data-efficient image transformers & distillation through attention. In *ICML*, 2021. 2
- [66] Hugo Touvron, Matthieu Cord, and Hervé Jégou. Deit iii: Revenge of the vit. In *ECCV*, 2022. 2
- [67] Darren Tsai, Julie Stephany Berrio, Mao Shan, Eduardo Nebot, and Stewart Worrall. Ms3d: Leveraging multiple detectors for unsupervised domain adaptation in 3d object detection. In *International Conference on Intelligent Transportation Systems*. IEEE, 2023. 1
- [68] Narek Tumanyan, Assaf Singer, Shai Bagon, and Tali Dekel. Dino-tracker: Taming dino for self-supervised point tracking in a single video. In *Proceedings of the European Conference on Computer Vision*, 2024. 2
- [69] Ozan Unal, Dengxin Dai, and Luc Van Gool. Scribble-supervised lidar semantic segmentation. In *Proceedings of the IEEE/CVF Conference on Computer Vision and Pattern Recognition*, pages 2697–2707, 2022. 5
- [70] Yan Wang, Xiangyu Chen, Yurong You, Li Erran Li, Bharath Hariharan, Mark Campbell, Kilian Q Weinberger, and Wei-Lun Chao. Train in germany, test in the usa: Making 3d object detectors generalize. In *Proceedings of the IEEE/CVF Conference on Computer Vision and Pattern Recognition*, pages 11710–11720, 2020. 1
- [71] Zhiyu Wang, Li Wang, Liang Xiao, and Bin Dai. Unsupervised subcategory domain adaptive network for 3d object detection in lidar. *Electronics*, 10(8):927, 2021.
- [72] Maciej K Wozniak, Mattias Hansson, Marko Thiel, and Patric Jensfelt. Uada3d: Unsupervised adversarial domain

- adaptation for 3d object detection with sparse lidar and large domain gaps. *arXiv preprint arXiv:2403.17633*, 2024. 1
- [73] Maciej K Wozniak, Hariprasath Govindarajan, Marvin Klingner, Camille Maurice, B Ravi Kiran, and Senthil Yogamani. S3pt: Scene semantics and structure guided clustering to boost self-supervised pre-training for autonomous driving. In *Proceedings of the IEEE Winter Conference on Applications of Computer Vision*, 2025. 1, 2
- [74] Xiaoyang Wu, Xin Wen, Xihui Liu, and Hengshuang Zhao. Masked scene contrast: A scalable framework for unsupervised 3d representation learning. In *Proceedings of the IEEE/CVF Conference on Computer Vision and Pattern Recognition*, 2023. 2
- [75] Xiaoyang Wu, Li Jiang, Peng-Shuai Wang, Zhijian Liu, Xihui Liu, Yu Qiao, Wanli Ouyang, Tong He, and Hengshuang Zhao. Point transformer v3: Simpler faster stronger. In *Proceedings of the IEEE/CVF Conference on Computer Vision and Pattern Recognition*, 2024. 4, 5, 6
- [76] Xiaoyang Wu, Li Jiang, Peng-Shuai Wang, Zhijian Liu, Xihui Liu, Yu Qiao, Wanli Ouyang, Tong He, and Hengshuang Zhao. Point transformer v3: Simpler, faster, stronger. In *CVPR*, 2024. 7
- [77] Zhirong Wu, Shuran Song, Aditya Khosla, Fisher Yu, Lin-guang Zhang, Xiaou Tang, and Jianxiong Xiao. 3d shapenets: A deep representation for volumetric shapes. In *Proceedings of the IEEE/CVF Conference on Computer Vision and Pattern Recognition*, 2015. 2
- [78] Zhirong Wu, Yuanjun Xiong, Stella X Yu, and Dahua Lin. Unsupervised feature learning via non-parametric instance discrimination. In *CVPR*, 2018. 2
- [79] Aoran Xiao, Jiaxing Huang, Dayan Guan, Kaiwen Cui, Shijian Lu, and Ling Shao. Polarmix: A general data augmentation technique for lidar point clouds. *NeurIPS*, 2022. 2
- [80] Aoran Xiao, Jiaxing Huang, Weihao Xuan, Ruijie Ren, Kangcheng Liu, Dayan Guan, Abdulmotaleb El Saddik, Shijian Lu, and Eric P Xing. 3d semantic segmentation in the wild: Learning generalized models for adverse-condition point clouds. In *Proceedings of the IEEE/CVF Conference on Computer Vision and Pattern Recognition*, pages 9382–9392, 2023. 5
- [81] Saining Xie, Jiatao Gu, Demi Guo, Charles R Qi, Leonidas Guibas, and Or Litany. Pointcontrast: Unsupervised pre-training for 3d point cloud understanding. In *Proceedings of the European Conference on Computer Vision*, 2020. 2
- [82] Qiangeng Xu, Yin Zhou, Weiyue Wang, Charles R Qi, and Dragomir Anguelov. Spg: Unsupervised domain adaptation for 3d object detection via semantic point generation. In *Proceedings of the International Conference on Computer Vision*, pages 15446–15456, 2021. 1
- [83] Xiang Xu, Lingdong Kong, Hui Shuai, Wenwei Zhang, Liang Pan, Kai Chen, Ziwei Liu, and Qingshan Liu. 4d contrastive superflows are dense 3d representation learners. *arXiv preprint arXiv:2407.06190*, 2024. 2, 3, 4, 5, 7, 8
- [84] Xiang Xu, Lingdong Kong, Hui Shuai, Liang Pan, Ziwei Liu, and Qingshan Liu. Limoe: Mixture of lidar representation learners from automotive scenes. *Proceedings of the IEEE/CVF Conference on Computer Vision and Pattern Recognition*, 2025. 2, 3, 5, 7
- [85] Jihan Yang, Shaoshuai Shi, Zhe Wang, Hongsheng Li, and Xiaojuan Qi. St3d: Self-training for unsupervised domain adaptation on 3d object detection. In *Proceedings of the IEEE/CVF Conference on Computer Vision and Pattern Recognition*, pages 10368–10378, 2021. 1
- [86] Jihan Yang, Shaoshuai Shi, Zhe Wang, Hongsheng Li, and Xiaojuan Qi. St3d++: Denoised self-training for unsupervised domain adaptation on 3d object detection. *IEEE Transactions on Pattern Analysis and Machine Intelligence*, 45(5): 6354–6371, 2022. 1
- [87] Junbo Yin, Dingfu Zhou, Liangjun Zhang, Jin Fang, Cheng-Zhong Xu, Jianbing Shen, and Wenguan Wang. Proposal-contrast: Unsupervised pre-training for lidar-based 3d object detection. In *Proceedings of the European Conference on Computer Vision*, 2022. 2
- [88] Xumin Yu, Lulu Tang, Yongming Rao, Tiejun Huang, Jie Zhou, and Jiwen Lu. Point-bert: Pre-training 3d point cloud transformers with masked point modeling. In *Proceedings of the IEEE/CVF Conference on Computer Vision and Pattern Recognition*, 2022. 2
- [89] Jiakang Yuan, Bo Zhang, Xiangchao Yan, Tao Chen, Botian Shi, Yikang Li, and Yu Qiao. Bi3d: Bi-domain active learning for cross-domain 3d object detection. In *Proceedings of the IEEE/CVF Conference on Computer Vision and Pattern Recognition*, pages 15599–15608, 2023. 1
- [90] Hao Zhang, Feng Li, Xueyan Zou, Shilong Liu, Chunyuan Li, Jianwei Yang, and Lei Zhang. A simple framework for open-vocabulary segmentation and detection. In *Proceedings of the International Conference on Computer Vision*, 2023. 2, 3
- [91] Renrui Zhang, Liuhui Wang, Yu Qiao, Peng Gao, and Hongsheng Li. Learning 3d representations from 2d pre-trained models via image-to-point masked autoencoders. In *Proceedings of the IEEE/CVF Conference on Computer Vision and Pattern Recognition*, 2023. 2
- [92] Yifan Zhang and Junhui Hou. Fine-grained image-to-lidar contrastive distillation with visual foundation models. *Advances in Neural Information Processing Systems*, 2024. 2, 3, 8
- [93] Yifan Zhang and Junhui Hou. Is contrastive distillation enough for learning comprehensive 3d representations? *arXiv preprint arXiv:2412.08973*, 2024. 3, 8
- [94] Yifan Zhang and Junhui Hou. Fine-grained image-to-lidar contrastive distillation with visual foundation models. *Advances in Neural Information Processing Systems*, 2024. 3
- [95] Zaiwei Zhang, Rohit Girdhar, Armand Joulin, and Ishan Misra. Self-supervised pretraining of 3d features on any point-cloud. In *Proceedings of the International Conference on Computer Vision*, 2021. 2
- [96] Jinghao Zhou, Chen Wei, Huiyu Wang, Wei Shen, Cihang Xie, Alan Yuille, and Tao Kong. Image BERT pre-training with online tokenizer. In *ICLR*, 2022. 2

## Supplementary Material

### A1. Additional Experiments

We use the Mix3D [52] augmentation during pre-training and show an ablation study for this choice in Tab. 9. We find that Mix3D provides a modest performance boost. For pre-training both ScaLR and our CleverDistiller we use the Mix3D augmentation.

Mix3D	nuScenes		KITTI	Waymo
	LP	1%	1%	1%
✗	48.95	55.36	49.03	50.09
✓	49.81	56.90	50.59	50.99

Table 9. Ablation study of Mix3D during distillation

### A2. Class-wise results

In Sec. A2 we compare the class-wise performance of CleverDistiller with other methods after finetuning on 1% of the training data. We generally outperform other methods, including the most recent LiMoE on most classes Sec. A2.

### A3. Qualitative analysis of features

Similarity maps presented in Fig. 5 illustrate the segmentation ability of our pretrained model, CleverDistiller. The query points include “truck”, “car”, “driveable surface”, and “vegetation”. CleverDistiller shows strong semantic discriminative ability without fine-tuning, similar to features distilled from camera foundational models. This effectiveness can be attributed to three key aspects: 1) Cosine similarity loss, which ensures that features are aligned; 2) An MLP projection head that retains information during projections, unlike previous methods using linear layers, helping the features to become more aligned; 3) An additional 3D auxiliary spatial task that improves the 3D features and understanding of the 3D backbone. The visualization of feature similarities in Fig. 5 highlights how CleverDistiller’s features align with those of the teacher model. Rows 1 and 3 show similarities of query pixels to other pixels based on the teacher model’s image features, while rows 2 and 4 show similarities of query points to other points based on CleverDistiller’s distilled backbone features. Yellow denotes high similarity and blue denotes low similarity, with query points/pixels marked by red crosses. Best viewed in color.

<b>Method</b>	<b>mIoU</b>	<b>barrier</b>	<b>bicycle</b>	<b>bus</b>	<b>car</b>	<b>construction vehicle</b>			<b>motorcycle</b>	<b>pedestrian</b>	<b>traffic cone</b>	<b>trailer</b>	<b>truck</b>	<b>driveable surface</b>	<b>other flat</b>	<b>sidewalk</b>	<b>terrain</b>	<b>manmade</b>	<b>vegetation</b>
<b>ViT-S</b>																			
SLidR	41.2	0.0	0.0	26.6	72.0	12.4	15.8	51.4	22.9	11.7	35.3	92.9	36.3	58.7	63.6	81.2	82.3		
Seal	44.3	20.0	0.0	19.4	74.7	10.6	45.7	60.3	29.2	17.4	38.1	93.2	26.0	58.8	64.5	81.9	81.9		
<b>CleverDistiller50</b>	53.7	59.1	0.0	61.4	83.4	1.2	40.1	62.1	23.1	28.0	56.3	93.7	53.3	62.2	68.8	83.5	82.6		
ScaLR	53.0	58.4	0.0	64.9	83.3	10.5	20.7	59.6	24.6	26.4	55.8	93.9	51.2	63.4	68.5	83.7	83.1		
SuperFlow	47.8	38.2	1.8	25.8	79.0	15.3	43.6	60.3	0.0	28.4	55.4	93.7	28.8	59.1	59.9	83.5	83.1		
LiMoE	49.6	39.9	4.6	27.3	80.2	17.1	45.4	61.2	6.2	29.5	58.4	94.0	34.2	62.3	64.6	84.1	84.5		
<b>CleverDistiller100</b>	56.9	60.2	0.0	71.2	84.9	11.8	47.1	65.1	26.6	31.4	61.7	94.2	54.1	64.9	69.5	84.2	83.5		
<b>ViT-B</b>																			
PPKT	40.9	0.0	0.0	24.5	73.5	12.2	7.0	51.0	13.5	15.4	36.3	93.1	40.4	59.2	63.5	81.7	82.2		
SLidR	41.6	0.0	0.0	26.7	73.4	10.3	16.9	51.3	23.3	12.7	38.1	93.0	37.7	58.8	63.4	81.6	82.7		
Seal	46.0	43.0	0.0	26.7	81.3	9.9	41.3	56.2	0.0	21.7	51.6	93.6	42.3	62.8	64.7	82.6	82.7		
<b>CleverDistiller50</b>	55.8	60.7	0.0	68.8	85.1	22.0	28.9	61.8	27.6	30.1	61.0	94.0	52.9	63.7	69.1	84.0	82.9		
SuperFlow	48.1	39.1	0.9	30.0	80.7	10.3	47.1	59.5	5.1	27.6	55.4	93.7	29.1	61.1	63.5	82.7	83.6		
ScaLR	55.8	60.8	0.0	69.7	85.1	20.4	30.6	60.8	27.8	29.5	58.1	94.2	55.6	64.3	69.3	84.1	83.1		
LiMoE	50.2	41.5	3.8	32.2	81.7	12.9	49.3	61.1	7.3	29.3	57.8	94.2	35.1	62.9	65.4	84.0	84.8		
<b>CleverDistiller 100</b>	59.8	61.8	0.0	72.8	85.7	35.2	49.6	65.4	33.6	32.9	62.6	94.5	59.5	65.6	69.5	84.7	83.5		
<b>ViT-L</b>																			
PPKT	42.1	0.0	0.0	24.4	78.8	15.1	9.2	54.2	14.3	12.9	39.1	92.9	37.8	59.8	64.9	82.3	83.6		
SLidR	42.8	0.0	0.0	23.9	78.8	15.2	20.9	55.0	28.0	17.4	41.4	92.2	41.2	58.0	64.0	81.8	82.7		
Seal	46.3	41.8	0.0	23.8	81.4	17.7	46.3	58.6	0.0	23.4	54.7	93.8	41.4	62.5	65.0	83.8	83.8		
<b>CleverDistiller 50</b>	56.7	63.4	0.0	69.7	85.4	19.3	29.4	62.1	30.4	31.9	62.4	94.3	56.2	65.3	70.0	84.1	83.0		
SuperFlow	50.0	44.5	0.9	22.4	80.8	17.1	50.2	60.9	21.0	25.1	55.1	93.9	35.8	61.5	62.6	83.7	83.7		
LiMoE	51.4	45.3	4.1	25.3	82.2	18.4	52.5	61.8	22.3	26.4	56.2	94.3	37.6	63.3	63.9	84.4	85.0		
ScaLR	55.8	65.0	0.0	68.7	85.3	15.9	27.7	61.4	28.3	31.0	61.8	94.2	51.6	64.6	70.0	84.1	83.0		
<b>CleverDistiller 100</b>	60.6	65.5	0.0	72.3	88.3	37.2	37.4	65.1	35.3	40.9	71.9	94.5	55.8	66.5	70.6	85.0	83.8		

Table 10. Per-class IoU scores of state-of-the-art pretraining methods pretrained and fine-tuned on nuScenes with 1% annotations. All IoU scores are given in percentage (%).



Figure 5. Visualization of feature similarities of CleverDistiller. Rows 1 and 3 show similarities of query pixel to other pixels based on teacher model’s image features. Rows 2 and 4 show similarities of query point to other points based on the distilled backbone’s features. Best viewed in color. The query points / pixels are denoted using red crosses. Yellow denotes high similarity and blue denotes low similarity.